Time-resolved in-situ dislocation density evolution during martensitic transformation by high-energy-XRD experiments: A study of C content and cooling rate effects

Juan Macchi, Guillaume Geandier, Julien Teixeira, Sabine Denis, Frédéric Bonnet, Sébastien Allain

Time-resolved dislocation density evolution during martensitic transformation tracked in situ by High-Energy XRD experiments: a study of C content and cooling rate effects

Authors:
Juan Macchi[1], Guillaume Geandier[1], Julien Teixeira[1], Sabine Denis[1], Frédéric Bonnet[2], Sébastien Y.P Allain[1]

[1] Institut Jean Lamour, UMR 7198 CNRS Université de Lorraine, Campus ARTEM Nancy, France

[2] ArcelorMittal Maizières Research SA, Voie Romaine, BP 30320, 57283 Maizières les Metz, France

Keywords: Steel ; Martensite ; Synchrotron ; X-Ray analysis ; Dislocation density ; Mechanical behavior

Corresponding author: Macchi, Juan
juan.macchi@univ-lorraine.fr
Tel.: +33 07 66 52 30 71
Postal address: Campus Artem, 2 allée André Guinier, 54011 Nancy

Abstract

Recent studies on the mechanical behavior of martensitic steels show the importance of considering lath martensite as a "polycrystalline aggregate" with a large distribution of the local yield strength. The latter depends on local microstructural features, such as lath sizes, carbon distribution (in solid solution, segregated to defects, in carbides) and density of defects Internal stresses have to be considered as an additional contribution to the yield strength participating to enlarge the distribution of the local flow stresses at the microstructure scale.

This study focuses on one of these microstructural features, the dislocation density. Its evolution is followed in situ upon martensitic transformation by High Energy X-Ray Diffraction experiments on a synchrotron beamline. A previously introduced method, based on modified Williamson-Hall (mWH) analysis, is improved in order to take account of the martensite lattice tetragonality when applying the mWH method.

The influence of the steel carbon content (0.11, 0.21 and 0.31 wt.% C steels) and of the cooling rate (-10, -50, -100 °C/s and water-quench) on the dislocation density evolution in martensite during the martensitic transformation is established. The effect of the cooling rate on the dislocation density is low between -10 and -100°C/s, but becomes visible after the water-quench. The higher the C content, the higher the dislocation densities at the end of the transformation. The steels with higher C content also show a wider distribution of the local dislocation density and, therefore, of the local yield strength.

Graphical abstract

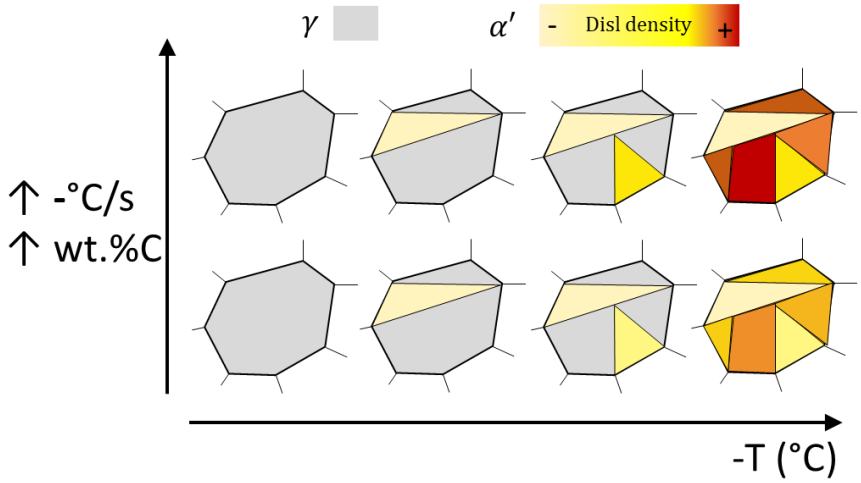

Highlights

- The evolution of the dislocation densities along with the martensitic transformation of three steels with different carbon compositions has been determined thanks to time-resolved in situ HEXRD experiments during quenching and post-mortem TEM and EBSD.

- A new method has been set to deconvolute the diffraction peak enlargement due to the defects and the one due to the possible tetragonality of the lattice.
- The dislocation densities well as the width of their distribution in the microstructure at room temperature increase with the cooling rate and with the carbon content, explaining the observed mechanical behavior of these steels.

Introduction

Martensite in steels is a hard phase that has been used by humanity during millennia [1] and it is still used as a versatile constituent of 3rd generation steels and in Press-Hardened Steels, both applied in the automotive industry among others [2]. This Body-Centered phase formed by a displacive transformation from the Face-Centered Cubic phase austenite presents a set of unique features as: a nano-scale hierarchized microstructure (laths, blocks and packets in the case of lath martensite [3] and nano-twins in high-carbon plate martensite [4]), carbon-trapped related tetragonality [5] (lately discussed by Maugis in [6]), an elevated density of microstructural defects (mainly dislocations and twins), and internal stresses as consequence of the transformation strain [7].

Regarding the mechanical properties of the martensite, different models can be found in the literature [8–10] to calculate its yield strength. These models take into account and describe the hardening mechanisms related to microstructure features, from Peierls barrier and substitutional and interstitial hardening to size hardening. An important contribution is the forest dislocation hardening as martensitic steels contain density of dislocations above 10^{15} $1/m^2$, as those found in severely deformed ferritic steels. It thus gives crucial importance to the proper determination of these densities of dislocations. Several methods can be found in the literature for their determination (Transmission Electron Microscope TEM, Electron Backscatter Diffraction EBSD, Neutron Diffraction ND, X-Ray Diffraction XRD and High Energy XRD) and many studies have highlighted that the mean density of dislocations in martensitic steels increases with the carbon content [11–19].

Recently the transformation sequence and its effects on the distribution of microstructural characteristics has gained relevance among the authors studying martensite [20]. The distribution of the microstructural features (thick/thin laths, higher/lower degree of self-tempering, lower/higher internal stresses, higher/lower dislocation densities) has as consequence a distribution of the local strength of the constituting microstructure features (laths, blocks and packets). It explains why recent studies on the behavior of martensitic steels have highlighted the importance of considering martensite not as an homogeneous phase but as a polycrystalline aggregate, a composite, at the scale of the laths or the blocks.

The resulting flow stress distribution function is the basis of the Continuum-Composite Approach (CCA) [21], and following models as the one developed by Wang et al. [22] including also the distribution of internal stresses. The main asset of the CCA models and its derivatives is the prediction of the whole stress-strain curves, not only the yield strength (YS). It consists in considering the work-hardening of martensitic steels as the result of an extended elasto-plastic transition as in the seminal Masing's model. In both mentioned models, the flow

stress distribution is presupposed without any quantitative relations with the microstructural components In a previous work, the present authors showed that the distribution of dislocation density and its distribution of strengthening through a forest hardening law are one of the main contributions to the flow stress spectrum [23]. In the present work yield strength is defined as the distance of the yielding surface to the no-stresses center, while the flow stress is the stress required to reach the yielding surface. In the case that no internal stresses are present the yield strength is equal to the flow stress, while they would differ in the presence of internal stresses.

A method to estimate the above-mentioned dislocation density distribution was developed and presented by the present authors in a previous work in a 0.21 wt.% C steel [23]. It is based on the exploitation of a modified Williamson-Hall (mWH) analysis [24] on in situ HEXRD experiments. It is improved in the present study in order to take account of the martensite lattice tetragonality when applying the mWH method. Even if the mean dislocation density values as function of the C content are found in the bibliography, no studies were found regarding the effect of the C content on the above-mentioned spectrum of dislocation densities, as far as its shape and width are concerned. The present work is focused on the effect of the C content on the evolution of dislocation density, as well as on its spatial distribution, during the martensitic transformation on three industrial low-carbon steels; 0.11, 0.21 and 0.31 wt.% C. The effect of the cooling rate is analyzed in situ by applying three different cooling rates under the martensite start temperature (Ms) for each studied steel. Quenching into water is considered in additional ex situ HEXRD experiments.

Methods

Steel composition

Three industrial low-carbon alloyed steels, provided by ArcelorMittal Maizières Research Center, France, with the composition presented on Table 1 were investigated. The samples were received after the cold-rolling stage, and then milled to a thickness around 1 mm.

Table 1: Chemical composition of the three studied steels.

Steel	C (wt.%)	Mn (wt.%)	Si (wt.%)	Cr (wt.%)	B (ppm)	Fe
0.1C	0.108	2.10	0.22	0.03	3	Balance
0.2C	0.210	1.82	0.25	0.18	4	Balance
0.3C	0.310	0.71	0.35	0.51	0	Balance

Even if Mn and Cr present variations between the chemical composition of the different steels (Table 1), their effect on the dislocation density is expected to be much lower than the effect of the C variation. As shown by [13], the mean dislocation densities in martensitic steels are related to the volume change associated with the displacive transformation. These authors

have also shown that interstitial elements produce a higher effect on the volume change than substitutional elements.

HEXRD set-up

In situ High Energy X-ray Diffraction (HEXRD) experiments were performed at the Deutsche-Elektronen-Synchrotron (DESY, PETRA-III) P07 beamline with a monochromatic beam. The energy of 87.1 keV (λ=0.014235 nm) allowed to work in transmission mode. The fast martensitic transformation was followed thanks to a 2D Perkin-Elmer detector enabling high acquisition rates (10 Hz). At the fastest applied cooling rate (-100 °C/s), a maximum martensite fraction of 10 wt.% could be formed between two acquisitions just below the Ms temperature. The temperature decrease between these two measurements is around 10°C as an image is taken by the detector every 0.1s. A better resolution (in terms of fraction) is obtained for lower cooling rates and for temperatures lower than the respective Ms of the steels (as the transformation kinetics are reduced).

The detector was positioned about 1.5 m behind the sample, giving access to full Debye-Scherrer rings with a maximum 2θ angle of 8° (5 Debye Scherrer rings per phase).

All the data utilized in the present work have been made public in [25].

Heat treatments

The heat treatments were performed with a modified Bähr DIL805 A/D dilatometer available on the beamline. For each steel, a set of three different heat treatments were applied. The heat treatments, consist of an austenitization stage (heating at 20 °C/s up to 880 °C then an isothermal holding of 300s) followed by a fast cooling (-100 °C/s) down to some degrees above Ms in order to avoid any time-dependent transformations (ferrite/pearlite/bainite). Then, below this temperature, three different cooling rates were applied: -10, -50 and -100 °C/s. In Figure 1, the demanded and measured temperature-time cooling curves are shown for the 0.31 wt.% C steel. A good agreement between requested and measured temperature is obtained (for the -100 °C/s and -50 °C/s experiments a deviation is however found from 100 °C down to room temperature during quenching). The austenitization heat treatment leads to mean prior austenite grain sizes of 10.5, 6.5 and 4 µm for 0.11, 0.21 and 0.31 wt.% C steel respectively. These values have been determined by Prior Austenite Grain reconstruction using Decrypt® software [26] on the basis of EBSD maps (results not shown here). For the studied heat treatments, more than 300 diffraction patterns have been acquired between the Ms temperature of the alloys and the room temperature for the slowest cooling rate (-10 °C/s) and around 35 for the fastest cooling rate (-100 °C/s). The Ms were determined by previous HEXRD experiments and Rietveld analysis as well as by dilatometric analysis. The Ms measured by dilatometry are 432, 407 and 382 ± 5 °C for 0.11, 0.21 and 0.31 wt.% C steels respectively by the method presented by Yang et al. [26] while the values obtained by HEXRD are 426, 372 and 342 ± 10 °C. The chosen criterion to determine the Ms by HEXRD

corresponds to a transformed fraction of 2 wt.%. This critical value is twice higher than the uncertainty of this measurement and thus above a realistic detection limit. A discussion of these Ms values and the comparison with the calculated ones is presented in Appendix A.

In addition, water quenched martensitic samples for each composition were produced in a laboratory furnace. The austenitization stage (heating at 0.1 °C/s up to 880 °C with an isothermal holding of 300s) is followed by a quench into water. The cooling rate measured during the quench for the three samples with welded thermocouple was between -1000 and -5000 °C/s. The samples, noted as WQ in the following, were roughly polished in order to remove surface oxides and then characterized post mortem.

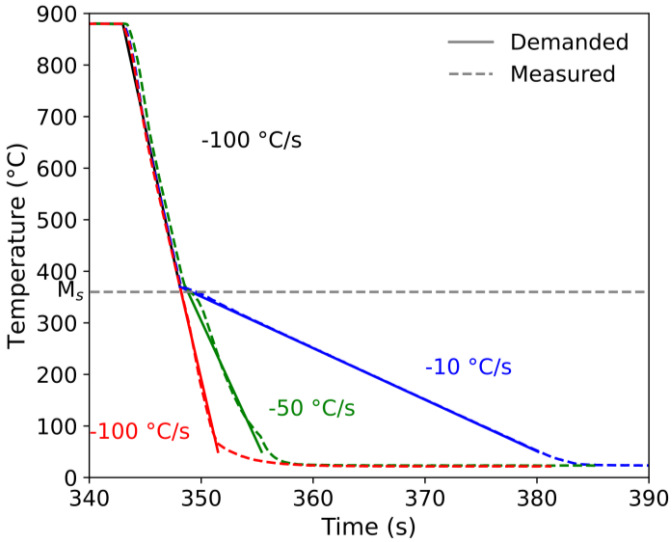

Figure 1: Schematic representation of the three cooling thermal paths applied at each steel and measured temperature-time curves for the 0.3C steel (Color online).

Rietveld analysis

The 2D diffraction patterns produced during the experiments were analyzed as in a previous work published by the authors [23]. First a circular integration was applied [27]; the deduced 1D diffractograms (Intensity vs 2θ) were analyzed systematically with a Rietveld refinement [28] to obtain phase fractions (the uncertainty is estimated around ±1% on the absolute value) as a function of time For the higher-carbon steel (0.3C), at the end of the cooling, the presence of transition carbides was inferred for the gas quenched samples where cooling rate below Ms is relatively small (the water quenched sample do not present any diffraction peaks which are characteristic of transition carbides). However, the intensity of their respective peaks was too weak and not sufficiently defined to be able to measure the fraction (less than 0.1wt.% presumably). As a consequence only two phases were considered during the analysis: austenite with a cubic face centered structure (Fm-3m) and martensite with a body centered tetragonal structure (I/4 mmm).

Single peak fitting method

The modified Williamson-Hall (mWH) method allows to deconvolute the coherent domain size from the dislocation density contributions on the Full Width at Half Maximum (FWHM) in anisotropic crystalline materials. The method was applied to estimate the dislocation density in martensite all along the cooling sequence. The peaks analyzed are {200}, {211}, {220} and {321}. The diffraction peaks were individually fitted with a single symmetric Pearson VII function, obtaining the position and the FWHM for each. The method will thus be called single peak fitting method in the following.

The peak broadening can be described by the following equation:

$$\Delta K = \frac{\zeta}{D} + \left(\left(\frac{\pi M b^2}{2}\right)^{1/2} \bar{\rho}^{1/2}\right) * K\overline{C_{hkl}}^{1/2} + OK^2\overline{C_{hkl}} \quad (1)$$

where ΔK=FWHM(θ)*2cos(θ))/λ , K is the scattering vector defined by K=2sin(θ)/λ, D is the crystallite size, M is a parameter depending on the dislocation density, b is the Burgers vector, $\bar{\rho}$ is the mean dislocation density and $\overline{C_{hkl}}$ is the average contrast factor of dislocations for the specific reflection. $OK^2\,\overline{C_{hkl}}$ is a higher order term with no meaning established [29], where O is much smaller than the coefficient before $K\overline{C_{hkl}}^{1/2}$, and it will not be considered here [30]. For the present work ζ was set equal to 0.9 as done in [31] and b (the Burgers vector) to 2.5 10^{-10} m. M is a dimensionless parameter linked to the outer cut-off radius of the dislocations and the dislocation arrangement inside the phase, it is set at 2.2 considering the average value from [16]. The average contrast factors ($\overline{C_{hkl}}$) as function of temperature were calculated as in the previous authors work [23]. The dislocation contrast factors at room temperature considering a ratio of 50% edge and 50% screw type dislocations are presented in Table 2.

Table 2: Dislocation contrast factors at room temperature considering a ratio of 50% edge and 50% screw type dislocations. Calculations according to ANIZC [32].

Ferrite	**{200}**	**{211}**	**{220}**	**{321}**
$\overline{C_{hkl}}$	0.278	0.141	0.141	0.141

The procedure described above (single peak fitting method) is developed for the description of perfectly cubic lattice. However, as said above, our martensitic microstructure are probably not cubic, but slightly tetragonal in a very limited extent. The tetragonality will lead to the weak dissociation (degeneration outbreak) of certain peaks from the cubic lattice and to a specific enlargement of these peaks even if a splitting is not observed strictly. As a consequence, the determination procedure based on the FWHM could be affected. This is the reason why, in the present work a new method (multiple function peak fitting) is proposed to deconvolute the contribution of the tetragonality by combining an analysis of the full diffractogram (Rietveld refinement) and of each peak individually.

Multiple peak fitting method

The multiple function peak fitting aims to fit each diffracting peak not by a single mathematical function but by different symmetric functions whose numbers correspond to the different reticular spacings associated to a degenerated family of planes. In the case of the family {200}, if the lattice is tetragonal, the (002) and the (200)/(020) planes have indeed two different reticular spaces and as a consequence two functions will be used (left in Figure 5), .In the case of the family {321} three mathematical functions will be used in the fitting (right in Figure 5) procedure. The red lines are the experimental data, the yellow, green and pink are the different functions used and the black ones are the sum of them.

To perform the multiple function peak fitting, the peak positions of respective functions and their respective intensity ratio have to be determined. To achieve this, a two-step method has been implemented.

Firstly, the c/a ratio is determined by the Rietveld refinement with a body centered tetragonal structure (I/4 mmm), then the reflection positions are calculated for each peak (i.e. in the case of {200}, the (002) and the (200)/(020) positions, while for the {321} three positions are calculated (321)/(231), (312)/(132) and (213)/(123)) with the Bragg's law. The angular separations, i.e. the difference between the mentioned positions, are then calculated.

Secondly, each diffraction peak (c.a. {200} or {321}) is individually modeled with the number of Pearson VII functions determined by the number of previously calculated positions (as for the single peak fitting method). The intensity ratio between Pearson VII functions used for each peak is obtained with the Bragg's analysis. In the case of {200} planes two functions are used, one twice intense than the other one corresponding to the (002) plane reflection. In this last step, the functions are forced to have the same FWHM and shape, and their position is restrained by the previously calculated angular separation. Finally, the obtained FWHM is used instead of the one-function-per-peak one. For the mWh, the mean angular position of the family is chosen as the intensity weighted average of the reflection positions. An example of the peaks modeled with the new method is presented in Figure 5.b.

It must be mentioned that the FWHM can be also affected by the possible distribution of hydrostatic internal stresses at the scale of the microstructure, as these stresses affect the lattice parameter following the law of linear elasticity [33] (isotropic bulk compressibility).

The effect of the possible distribution of internal stresses thus affects all the diffraction peaks and scale with the Braggs laws when considering the diffraction patterns. Nevertheless, it is not possible to deconvolute explicitly the contribution.

Microscopy

Transmission Electron Microscopy (TEM) was applied to obtain the dislocation density value of the 0.21 wt.% C steel at the end of a water quench and compared with the HEXRD mWH value. The sample was milled and polished mechanically unto a thickness around 100 μm

then 3 mm discs were punched from the slices. The discs were polished electrolytically with a solution of 2 butoxy-ethanol, methanol and perchloric acid with a Struers TecnuPol-5 twin-jet machine. The temperature of the solution was between 10 and 14 °C and a voltage of 40 V was applied. The electrolytic prepared sample were examined on a JEOL ACCEL-ARM200F microscope equipped with probe and image corrector. A cold FEG source working at an accelerating voltage of 200 keV on scanning mode was used for the TEM observations. Annular dark field images were used for the analysis, the thickness of the sample was determined by Energy-filtered transmission electron microscopy (EFTEM) measurements. The dislocation density was calculated with the equation presented by Morito et al.[13]. Six different sections were analyzed.

The EBSD study was conducted on a similar treated sample, water-quenched 0.21 wt.% C steel, to obtain the geometrically necessary dislocation (GND) density. The preparation consisted of sandpaper polishing until 4000 grit, diamond polished with 6, 3 and 1 µm grain size pastes and 30 minutes of final polishing with standard fumed silica suspension in order to remove any deformation introduced previously. The EBSD characterization was performed in a FEG-SEM Jeol 7001-F equipped with a Bruker e^- Flash HR EBSD detector. The following working conditions were followed: distance work of 12mm and an accelerating voltage of 15kV. The equation proposed by Liu et al. [34] to estimate the GND density was used with the Kernel Average Misorientation (KAM) angle, a square shape Kernel of 5*5pixels, the Burgers vector set to 2.5 10^{-10} m and the alpha parameter to 3. In the present work, 5 different zones were studied. The scan area on each sample was 60 x 45 µm, with a total surface around 13500 μm^2, a scanning step of 0.1 µm was used. The EBSD data was post-processed using AZtec Crystal Software.

Results

Phase transformation kinetics

The experimental cooling curve for the 0.2C steel cooled at -10 °C/s below Ms is presented in Figure 2 on which three temperatures are highlighted (380, 200 and 50 °C). The integrated diffractograms for the mentioned temperatures are shown on the right (the intensity is plotted in a logarithmic scale, a marker is shown each 50 measurement points), as well as the position for the diffracting planes in austenite and martensite. Martensitic peaks and the retained austenitic ones at the end of the treatments are obviously wider than the peaks of austenite before the transformation (even at lower temperatures).

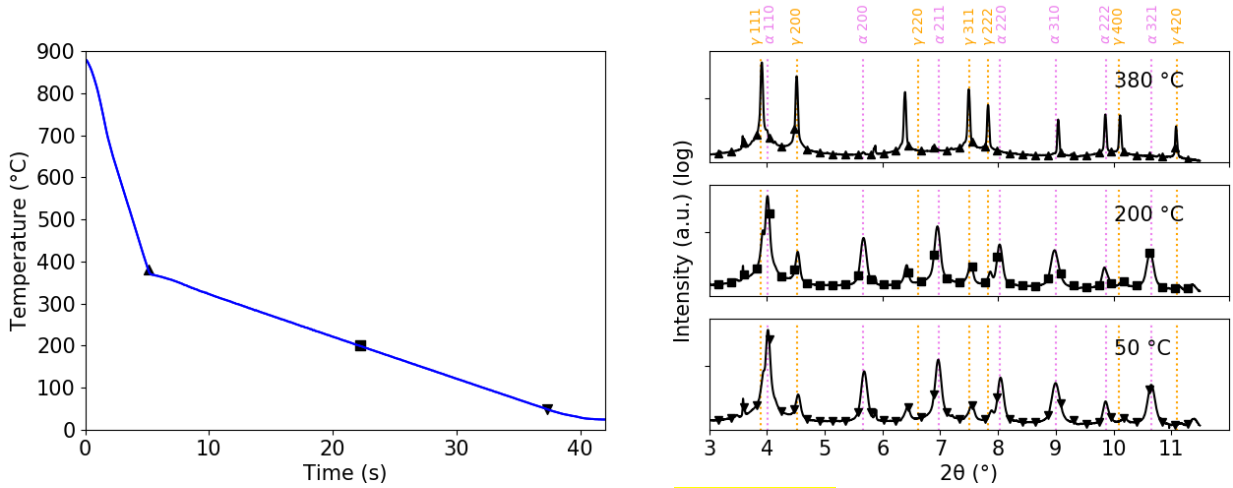

Figure 2: (a) Cooling curve of experiment carried out on the 0.2C steel cooled at -10 °C/s below Ms (b) Integrated 1D diffractograms recorded at the three temperatures highlighted in (a) and identified with symbols (triangle for 380 °C, square to 200 °C and inversed triangle for 50 °C). The diffracting position of the martensite are indicated as well as the ones of the austenite (Color online).

The phase transformation kinetics at the lowest cooling rate (-10 °C/s) below Ms for the three grades are represented in Figure 3.a. The results obtained with the two methods presented above are compared, i.e. the kinetics derived from the dilatometric signal and the results of the Rietveld refinement on the recorded diffractograms along the thermal treatment. For the sake of clarity, only one point each twenty is shown with a marker to distinguish the curves (two additional points have been added to the -100 °C/s curve in Figure 3.b, at 200 and 325 °C to facilitate the reading).

No previous body-centered phase is detected before the martensitic transformation, due to a completed austenitization and the high cooling rate (-100 °C) preventing diffusional transformations to occur. At the beginning of the martensitic transformations, the curves derived from the dilatometric signal show a sluggish stage followed by a faster regime for the 0.2C and 0.3C steels. The first step is too fast or inexistent for the lowest C content alloy. These two steps are often observed during dilatometer experiments and are related to the thermal gradients inherent from the technique (extremities of the sample are cooler than its center due the thermal pumping induced by the maintaining rods); the presence of decarburized layers and/or chemical heterogeneities in the specimen cannot however be totally ruled out too. As a consequence, the first stage is not representative of the mean bulk behavior of the material (which is revealed by HEXRD as the local analyzed volume is close to the control thermocouple). The Ms temperatures are 426, 372 and 342 ± 10 °C for 0.1C, 0.2C and 0.3C steel respectively considering the Rietveld refinement and are 432, 407 and 382 ± 5 °C if the dilatometric data are considered. A summary is given in Table 3. The comparison between the Ms determined by both methods and the calculated values from the literature is presented and is discussed in more details in Appendix A. The uncertainties of the HEXRD are ± 10 °C in the x axis at -10 °C/s, and 1 wt.% in y axis, one example for the 0.1C curve is shown at 404 °C.

Table 3: Ms temperatures determined by HEXRD (± 10 °C) and dilatometry (± 5 °C) for the three studied steels.

Steel	Ms by HEXRD (°C)	Ms by dilatometry (°C)
0.1C	426	432
0.2C	372	407
0.3C	342	382

Below 70 wt.% of martensite, the fractions determined by both technics are in good agreement. Above that value, the martensite fractions obtained by the Rietveld refinement are higher than the ones determined by dilatometry. The differences may be due again to thermal heterogeneities.

Figure 3.b shows the transformation kinetics measured by HEXRD for the 0.3C steel at 3 different cooling rates. According the resolution in time and in fraction of the experiments, the curves are similar. No clear evidence of the cooling rate effect is found regarding the Ms transformation start. Nevertheless, the cooling rate seems to affect the fraction of retained austenite fraction at room temperature. The errorbars of the curves are presented for each curve in one point (lines in black), the uncertainties increase with the cooling rate.

The evolution of retained austenite fraction at room temperature for the different steels is shown in Table 4. As expected, the higher the carbon content of the steel, the higher the fraction of retained austenite, for the -10 °C/s cooling rate it varies from 2.6 to 6.7 wt.% for C varying from 0.11 to 0.31 wt.% C. The reported values confirm that the higher cooling rate is, the lower the fraction of retained austenite. The main explanation to the latter tendency is an increase of the chemical stabilization at lower cooling rates as discussed in Appendix B. It has to be pointed out that some of the values for the 0.1C alloy do not follow the mentioned tendency, however they are in the incertitude.

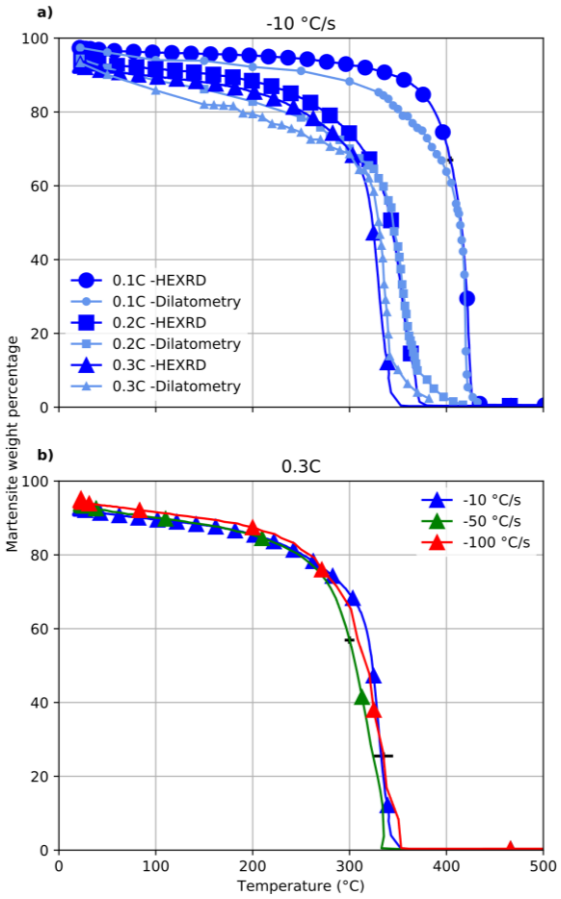

Figure 3: a) Martensite mass fraction as a function of temperature for the three studied steels at constant cooling rate below Ms (-10 °C/s) derived from the dilatometry and deduced from the Rietveld refinement. b) Martensite mass fraction as function of temperature for the 0.3C steel at three different cooling rates. The incertitudes of each curve in b) are presented observing a higher incertitude in the x axis increasing with the cooling rate. (Color online).

Table 4: Retained austenite at room temperature as function of C content and of cooling rate determined by Rietveld refinement (uncertainty equal to ± 1 wt.%).

	Cooling rate			
	-10 °C/s	**-50 °C/s**	**-100 °C/s**	**WQ**
0.1C	2.6	3.1	3.4	1.4
0.2C	5.6	4.9	4.1	1.8
0.3C	6.7	5.3	4.5	2.0

Dislocation densities: single peak fitting method

The evolution of the dislocation density in martensite as a function of the progress of the transformation (obtained with the original mWH method, single function method) for all nine studied conditions are presented in Figure 4.The results for each steel composition are displayed together to ease the comparison. The dislocation density increases for all the conditions with values between 1×10^{14} and 2×10^{15} $1/m^2$ at the beginning of the

transformation and reaches values between 1.2 x 10^{15} and 2.5 x 10^{15} $1/m^2$ at room temperature. The dislocation densities in the water-quenched samples at the end of the heat treatments are 1.5, 2.55 and 3.5 x 10^{15} $1/m^2$ for 0.1C, 0.2C and 0.3C steel respectively (black symbols in Figure 4). The estimation of the incertitude in the dislocation densities is complex due to the fact that the dislocation density is obtained by the slope of a linear fit based on points obtained by the fit of diffraction peaks with a distribution function. It has to be kept in mind that the parameter M of Eq.1 has been set constant while it may evolve during the experiment. To analyze the experimental incertitude, a set of experiments were performed in other synchrotron session with a different detector. The maximum ratio between the dislocation density herein presented and the one obtained in the supplementary experiments is 1 ± 0.25 at martensite fractions higher than 20 wt.%. At lower fractions a maximum of 4 is reached.

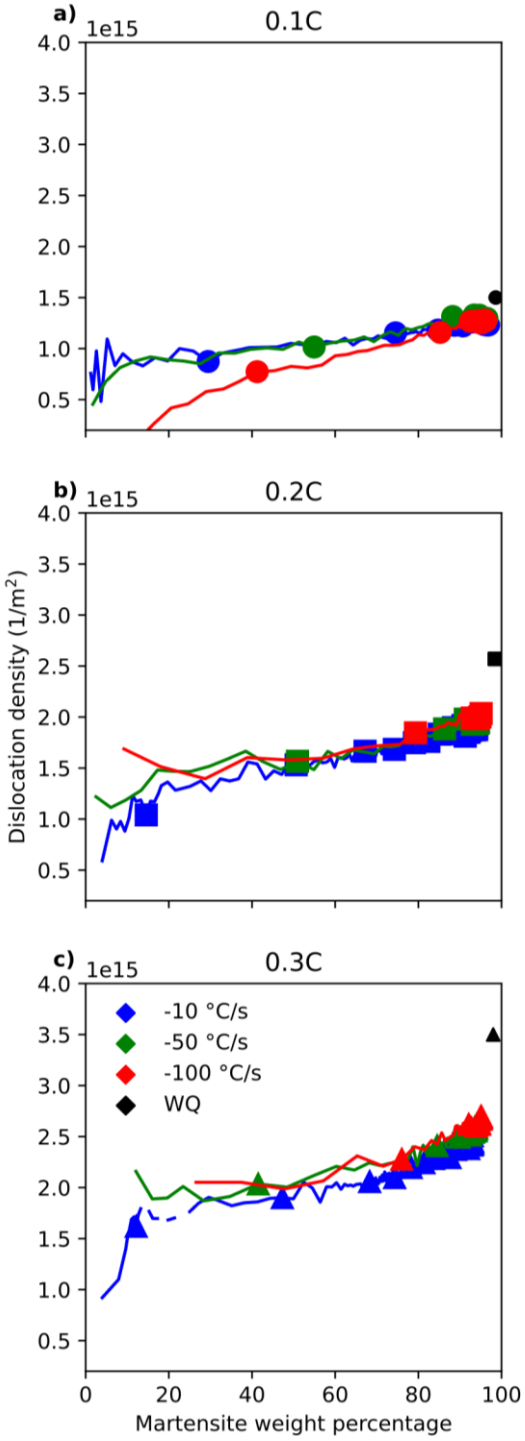

Figure 4: Dislocation density in martensite as function of the martensite mass fraction for the nine studied conditions as well as the dislocation density measured by HEXRD after water quench. (a) 0.1C steel (b) 0.2C steel (c) 0.3C steel. Blue, green and red curves corresponds to the different cooling rates studied in situ (-10°C/s, -50°C/s and -100°C/s respectively) and the black symbol to the post mortem determination after waterquenching (WQ). The 0.1C alloy results are indicated by circles, the ones of the 0.2C steel by squares and the ones of the 0.3C steel by triangles (Color online).

Dislocation densities: multiple peak fitting method

As explained above, the dislocation density determination by single peak fitting method can be affected by the tetragonality of the martensite

The new developed method to deconvolute the tetragonality is applied at room temperature results (where the tetragonality is higher) for the -100 °C/s condition for the three studied steels; the measured c/a ratio are respectively 1.0051, 1.0051 and 1.0077 determined by the Rietveld refinement for the 0.11, 0.21 and 0.31 wt.% C steel respectively.

The resulting diffractograms with the multiple peaks are presented in Figure 5. The black curves, sum of the individual Pearson VII functions, are well juxtaposed with the experimental one (red line). A small difference can be observed for the peak {200} around 5.7 2θ, due to an imposed asymmetry that is not observed in the mentioned peak. The values obtained using new the method are 1.25, 1.55 and 2.22 10^{15} $1/m^2$ while the ones using the one function per peak are 1.25, 2.0 and 2.45 10^{15} $1/m^2$ for 0.1C, 0.2C and 0.3C steel respectively. No difference is found for the lowest carbon steel. For the 0.2C steel the deconvoluted value is around 25% lower, and for the highest carbon steel the difference is around 10%.

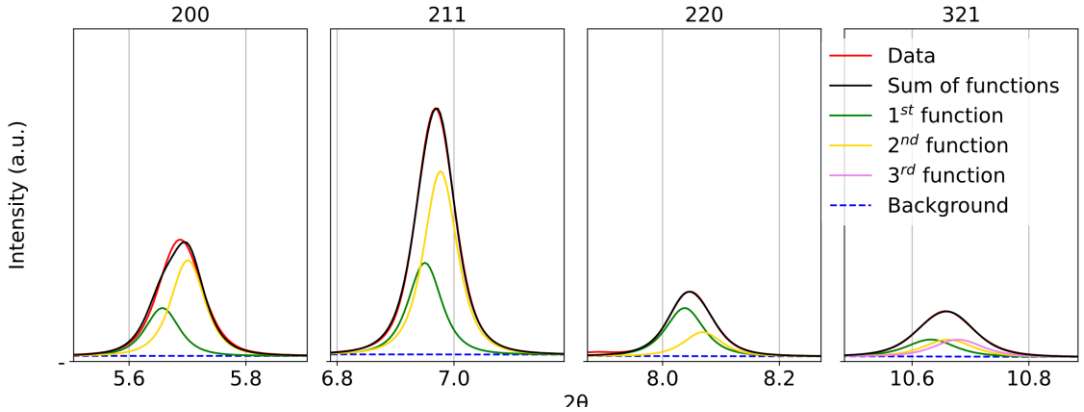

Figure 5: Room temperature experimental diffractograms of the 0.3C steel and modeled diffraction peaks following the multiple-function peak fitting, selected for the dislocation density determination (Color online).

Dislocation densities: TEM and EBSD

Figure 6 presents two micrographs obtained by TEM (a) and SEM-EBSD (b) respectively on the WQ 0.2C sample. Figure 6.a shows also the virtual lines used for the determination of the dislocation density. The total length of the lines is 2158 µm with a total number of intercepts of 77. The thickness of the sample determined by EFTEM is 90 nm (± 10 %). Figure 6.b shows a EBSD map composed by band contrast (sublayer on gray scale), high angle boundary (angle higher than 10°, marked with black lines) and KAM angle (scale from blue to green). The mean dislocation density in the water-quenched 0.2C steel was estimated to 9.5 x 10^{14} $1/m^2$ by TEM and the GND density to 1.3 x 10^{15} $1/m^2$ by EBSD. In the EBSD map, it seems obvious that the larger domains contains a lower dislocation density (blue). This last finding is in accordance with the work of Morsdorf et al. [20]. A summary of the obtained dislocation

densities at room temperature of the water-quenched condition of the three studied steels is presented in Table 5.

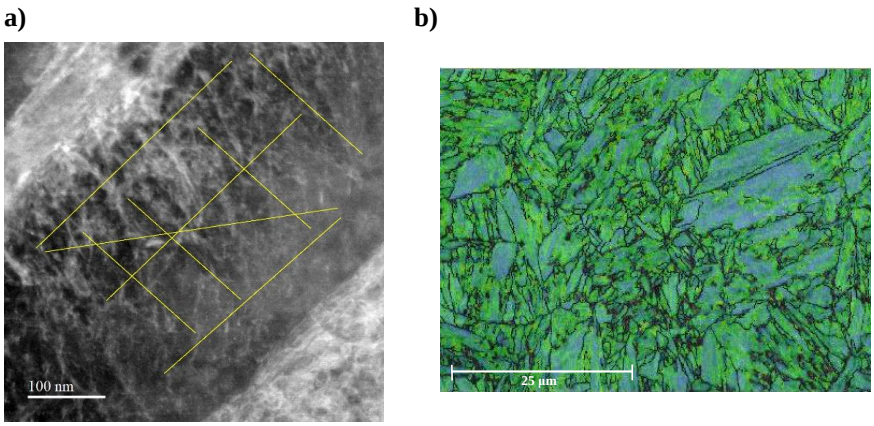

Figure 6: a) Dark field TEM micrograph of a martensite lath with the virtual lines used to measure the dislocation density in the WQ 0.21 wt.% C sample. b) Combined EBSD maps showing the band contrast, the high angle grain boundary and the KAM angle on the same sample (Color online).

Table 5: Dislocation densities of the water-quenched samples of the three studied steels by HEXRD, EBSD and MET.

Steel	**Dislocation density (10^{15} 1/m^2)**		
	HEXRD	**EBSD**	**TEM**
0.1C	1.5		
0.2C	2.5	1.3	0.95
0.3C	3.5		

Discussion

Dislocation densities at room temperature

The first important finding of these experiments and analyses is that the dislocation densities determined with the multiple peak fitting method are in some cases lower than the ones estimated by the reference single peak fitting method but not in a decisive way.

It can be concluded that the effect of the tetragonality on the presented determination of dislocation density by the single peak fitting method evaluation can be neglected. This result is sustained by the fact that the diffraction peak are highly symmetrical meaning that the possible tetragonality put into evidence by the Rietveld analysis is probably an upper bound. In the following, only the results obtained with the latter (more simple) method will be discussed.

Effect of the cooling rate and the carbon content

Figure 4 shows that the higher the cooling rate, the higher the density of dislocations (an exception if found for the 0.1C steel at the cooling rate -100 °C/s below Ms when the

martensite fraction is lower than 80 wt.%). Until 80 wt.% martensite, the curves are similar and the differences appear at lower temperatures. Nevertheless, for all continuous cooling experiments the mentioned tendency remains and is inside the amplitude of the measurement incertitude (at least 25% can be considered [23]). The water-quenched value is systematically and significatively higher than the other values, confirming more decisively the influence of the cooling rate on the dislocation density. If an incertitude of 25% is considered for the dislocation density of the WQ condition and also for the last point of the -100 °C/s condition the uncertainties are almost separated, justifying a phenomenon related to the cooling rate and not only a measurement incertitude. The same phenomena is found by Nishi et al. [35]. A lower recovery can be one of the explanations of a higher dislocation density in the faster cooled samples.

In order to assess the effect of the C content, the evolution of the dislocation density in the three steels for the lowest cooling rate (-10°C/s) is represented in Figure 7. The curves present a similar behavior for the three studied cases for martensite fractions higher than 20 wt.%; a continuous increase of the dislocation density is observed. The gap between the three curves increases gradually with the increase of the formed martensite. However, at lower fractions the behavior is different. For the three compositions the first dislocation densities values (where the incertitude is higher due to a lower definition of the diffracted peaks) are around the same value, between 0.5 and 1 x 10^{15} $1/m^2$. The higher dislocation density found in martensite with higher C content has been related to a higher volume expansion during the martensitic transformation from the face-centered phase to the body-centered phase [13]. As previously mentioned the incertitude can be estimated at 1 ± 0.25 times the value reported if the effect of the parameter M is not considered.

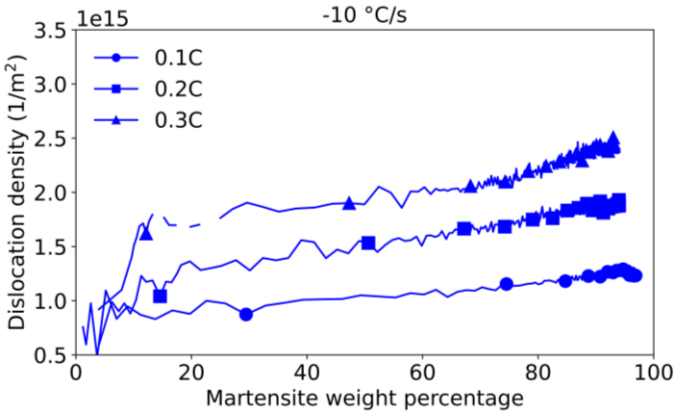

Figure 7: Effect of the C content of the steel on the dislocation density evolution with the mass fraction, at constant cooling rate (Color online).

The dislocation density of the 0.1C steel quenched at -10 °C/s increases at a low rate, only presenting a ratio close to 2 between the first determined value and the last one. Two main explanations can be postulated for this behavior. The first one is that a lower C content produces a lower volume change and, therefore, a lower increase of the dislocation density with the formed phase fraction. The second explanation is that the 0.1C steels suffers higher

relaxation/recovery phenomena due to its higher Ms temperature. A combination of both hypothesis cannot be ruled out.

Comparison with the literature

The dislocation densities determined for the three composition studied in the WQ condition by HEXRD as well as the dislocation densities for the WQ 0.21 wt.% C condition measured by EBSD and by TEM are presented in Figure 8 in comparison with values found in the literature by different characterization methods (TEM, EBSD, neutron diffraction (ND), XRD, Small-Angle Neutron Scattering (SANS)) [11–19]. The values obtained by the three characterization methods applied in the present work are clearly in the expected range of values and more interestingly the linear behavior obtained with the HEXRD values (density as a function of the carbon content) is similar to the one presented by [11,14,19].

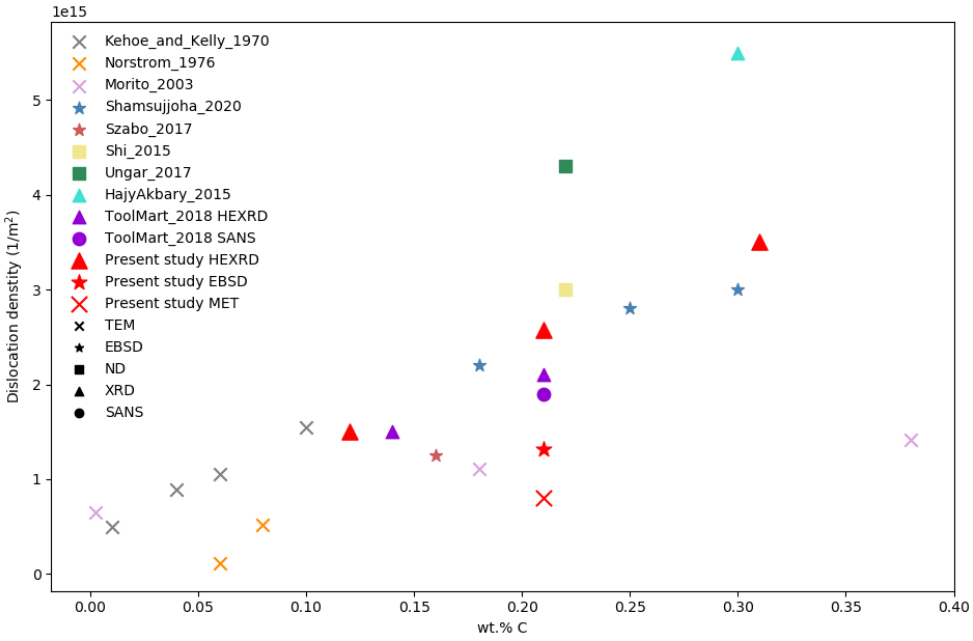

Figure 8: Comparison between the values obtained in the present study (red symbols) with the ones from the literature [11–19] (other colors). The values determined by TEM are indicated with a cross, those by EBSD by a star, those by neutron diffraction (ND) with a square, those by XRD by a triangle and the one by Small-Angle Neutron Scattering (SANS) with a circle (Color online).

Regarding the coherence between the values obtained by the different methods, the higher dislocation density estimated by XRD might be due to the lattice perturbations induced by other microstructures defects as twins, lath boundaries, small carbon heterogeneities producing different lattice parameter. The dislocation density determined by EBSD is low compared to the value obtained by HEXRD, but it only takes into account the GNDs, which represent only a fraction of the total density of defects.

The relative low dislocation density measured by TEM can be justified by the sample preparation, some relaxation/recovery may occur in the thin sample (image forces due to the proximity of free surface), as well as by a bias in the measurement. The determination have been done in regions in which the dislocations can be identified, however some other regions

might present higher dislocation densities which we were not be able to quantify. The boundaries rich in dislocations may have been also not fully considered by this last technic while HEXRD characterizations do not present this limitation.

Spatial distribution of dislocation densities

The evolution of the dislocation density along with the martensite transformation can be explained from a mathematical point of view either by an average increase of a uniform dislocation density or by the progressive formation of martensite with higher dislocation densities, while the previously formed martensite keeps its dislocation density constant. Intermediate scenario can also be considered but the second extreme case seems relevant in the case of the martensite transformation as it is supported by different experimental observations, in particular in the work of Morsdorf et al. [20]. This scenario was adopted by the authors in a previous work [23].

Under the main hypothesis that the formation of new martensite does not modify the dislocation density in the previously formed martensite, it is possible to calculate the local dislocation density in the new formed martensite. For a given formed martensite fraction (F), the mean dislocation density ($\bar{\rho}$) (the measured value) is equal to the average of the local dislocation densities that appeared in all previously formed martensite laths. This local dislocation density will be called ρ_{inst} in the following. In other words, each formed martensite fraction (f) has a local dislocation density (ρ_{inst}) giving at a given total formed martensite fraction (F) an average dislocation density ($\bar{\rho}$) that is the value measured. As a consequence, the mean density can be calculated as follows :

$$\bar{\rho} = \frac{1}{F}\int_0^F \rho_{inst}\,(f)df \qquad (3)$$

Deriving equation 3 with respect to F, the instantaneous dislocation density of the dislocations at F can be obtained by :

$$d\big(F\bar{\rho}(F)\big) = \rho_{inst}(F)dF \qquad (4)$$

As shown by equations 3 and 4, the only input required to calculate ρ_{inst} is the mean dislocation density as function of the martensite fraction. In order to avoid the inherent experimental fluctuations when measuring the transformed fraction, an empirical representation is proposed to describe $\bar{\rho}$ as function of F. The proposed equation is a parametrized square root formulae:

$$\bar{\rho} = A + B\sqrt{F} \qquad (5)$$

Even if the equation has been proposed only based on the search of an equation that can describe the tendencies observed, a first interpretation of the parameters A and B can be proposed. The parameter A can be related to the minimum dislocation density required to partially relax the internal stresses caused by the volume change during the martensitic transformation. The parameter B can be related to the slope of the evolution of the dislocation density with the martensite formed fraction, it might be affected by the C content (affecting the volume change [13]) and other factors as a possible recovery during the quench (this effect may be ruled out at high cooling rates).

The experimental mean dislocation density as function of the martensite fraction for the three studied compositions were modeled with equation 5 in order to obtain the required parameters (only the lowest cooling rate data were analyzed as thley are the best time resolved ones). The found values for parameter A are 6.32 x 10^{14}, 6.03 x 10^{14} and 9.02 x 10^{14} 1/m^2 for 0.11, 0.21 and 0.31 wt.% C steel respectively and the values for parameter B are 6.32 x 10^{14}, 1.28 x 10^{15} and 1.50 x 10^{15} 1/m^2 respectively. The experimental points as well as the calibrated curves are shown in Figure 9.a. Although the parameter A depends on the initial density at low martensite fraction in which the uncertainty is higher (giving a higher incertitude than for the parameter B), the herein presented values are in accordance with the dislocation density of the 0.0026 wt.% C martensite of the work of Morito et al. [13].

The adjustment quality increases with decreasing the C content. For the 0.31 wt.% C steel, the experimental values for less than 10 wt.% martensite formed are smaller than the fitted ones, however the resolution of diffraction peaks for low phase fraction is lower than for higher phase fractions. From 10 to 30 wt.% the experimental values are higher than the modelled ones, then a relative good correlation is found. Some of these discrepancies between the experimental values and the modelled ones could be avoided by considering a more complex equation, however the authors choice is to keep a simple equation with only 2 free parameters.

The instantaneous dislocation density curve for each steel composition was calculated with equation 4. They are shown in red in Figure 9.a. Note that the incertitude of the average dislocation densities would affect the calculated instantaneous dislocation density curves. If the average dislocation density is multiplied by a 1.25 ratio, then the final average dislocation density is calculated to be 3.9 × 10^{15} 1/m^2 for the 0.3C steel quenched at -10 °C/s (while the original value previously presented was 3.1× 10^{15} 1/m^2). Therefore, higher values of instantaneous dislocation densities would be found.

For the first formed martensite, the instantaneous dislocation density is equal to the parameter a previously set, however for the last formed martensite (considering a 100 % martensitic fraction) the instantaneous dislocation density is equal to 1.93 x 10^{15}, 3.43 x 10^{15} and 4.8 x 10^{15} 1/m^2 for 0.11, 0.21 and 0.31 wt.% C steel respectively. The first formed martensite at higher temperature presents a lower dislocation density than the one formed at lower temperature in an advanced state of the martensite transformation.

This evolution naturally generates a spatial distribution of dislocation density and consequently a "composite" microstructure. This heterogeneous spatial distribution of dislocations adds to the distributions of lath sizes or local compositions. On the whole, martensite must been seen as multiphase aggregate whose local flow stresses depends on these three latter microstructural features but also presumably on the internal stresses. All these contributions are presumably correlated but the literature is not definitive on this question. In the following, only the yield strength distribution due to dislocations will be analyzed and discussed.

The contribution to the local yield strength of the dislocations can be calculated by the Taylor equation[36]:

$$\sigma_{disl} = \alpha C_T \mu b \sqrt{\rho_{inst}} \quad (6)$$

where α is a geometrical constant set equal to 0.4, the Taylor factor (C_T) equal to 3, μ is the shearing modulus, b is the Burgers vector (2.5×10^{-10} m) and ρ_{inst} is the instantaneous dislocation density. The shear modulus is calculated as function of the chemical composition for each steel at room temperature, being equal 76.1, 75.5 and 75.0 GPa for 0.11, 0.21 and 0.31 wt.% C steel respectively [37].

The probability densities of finding a martensite fraction with a certain dislocation was calculated by applying equation 6 to the instantaneous dislocation densities. Applying the Taylor equation to the instantaneous dislocation densities allows to obtain the evolution of the dislocation hardening with the martensite fraction. The dislocation strengthening was calculated each 0.5 wt.% formed martensite, then fraction has been regrouped based on a 25 MPa binned grid of the dislocation strengthening. After normalization (force the integral of the curve to be equal to 1), the integral of the curve is the probability density of finding a martensite fraction with a certain dislocation strengthening. A similar method has been detailed in an authors' previous study [23]. The mentioned probabilities are presented in Figure 9.b for the three steel compositions.

The three probability densities curves of finding a martensite with a given dislocation density hardening have similar shapes as it is inherited from the shape of the instantaneous dislocation density curves. It can be observed that for the two steels with lower carbon content, the softer martensite has a similar dislocation density hardening, 590 MPa. This is a direct consequence of the similar obtained values of the parameter A in the equation 5. For the 0.3C steel, the value is a bit higher (710 MPa). In a previous study, Allain et al. showed that the minimum of the distributions of yield strength (corresponding to a microplasticity stage) required to model the tensile curve of martensite does not vary with the C content [21]. Our results agree for the two lower C content alloys. The higher value obtained for the 0.3C steel have to be thought-out considering the uncertainty due to the lower quality of the fit (as shown in Figure 9.a).

The maximal strengthening due to dislocation density found for the 0.1C steel is 890 MPa, while for the 0.2C steel this value is 1110 MPa and for the 0.3C steel it is 1250 MPa. The width of the distribution increases with the C content : (300, 520 and 540 MPa for 0.1, 0.2C and 0.3C steel respectively).

The Figure 9b presents the proportion of martensite as function of the dislocation density for the three C steels. For example, in the case of the 0.1C steel, the first formed martensite would have a dislocation contribution to its yield strength of ca. 600 MPa. The proportion of martensite fraction with a dislocation strengthening lower than 800 MPa is the integral of the presented curve between 0 and 800 MPa. The proportion of martensite presenting a given dislocation strengthening is the integral of the curve between a positive and negative differential around the selected dislocation hardening. In the case of the 0.1C steel the proportion of martensite with a dislocation strengthening higher than 950 MPa is zero while in the case of the 0.2C it is 64 % and in the case of the 0.3C steel it is 85 %.

If the fraction of martensite with a lower dislocation strengthening than a given value is to be calculated, then the integral of the probability curve between 0 and the mentioned value has to be calculated. For example, 40 % of the 0.1C martensite has a dislocation strengthening lower

than 800 MPa, while only 11 % of the 0.2C martensite and 2.5 % of the 0.3C martensite present a dislocation strengthening lower than 800 MPa.

The calculated instantaneous dislocation density as well as the distribution of dislocation strengthening are related to the hypothesis that the new formed martensite does not modify the dislocation density of the previously formed martensite. If some degree of deformation occurs in the previously formed martensite due to the transformation, then either the dislocation density stays almost constant or an increase of the dislocation density happens. As a consequence, the herein presented instantaneous dislocation density has a maximum distribution based on the measured dislocation density, their dispersion may be lower if the used hypothesis is not fully valid (i.e. some deformation happens in the previously formed martensite).

However, it can be concluded that our results are in agreement with those of Allain et al. [21] who showed that the presupposed dispersion of local yield strength needed to predict the tensile behavior increases with the C content. Meaning that the dislocation density hardening distribution is not only a contribution to the yield strength distribution but also it plays a key role in the increasing dispersion of it with the C content.

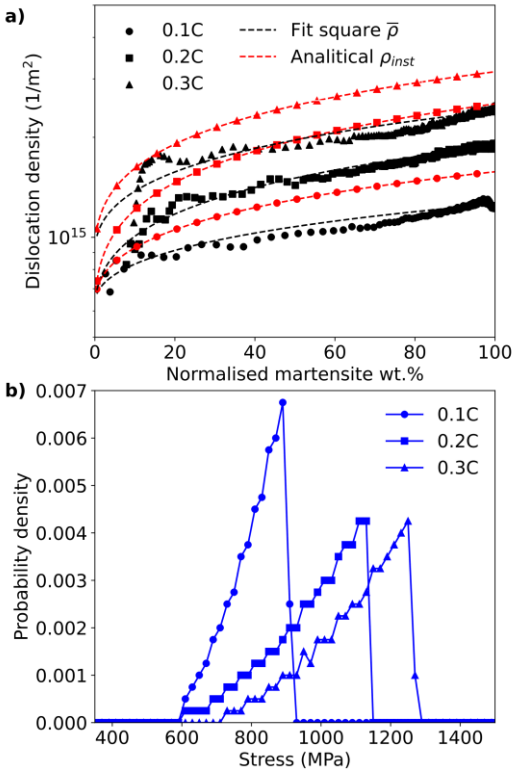

Figure 9: a) Experimental and modeled mean dislocation density as function of the martensite fraction. b) Probability density of finding a martensite fraction with a certain dislocation density strengthening for the three studied steels (Color online).

Conclusions

The dislocation densities evolutions in martensite during controlled martensitic transformation conditions were determined by the modified Williamson-Hall method from in-situ HEXRD

experiments for three low-carbon steels (0.11, 0.21 and 0.31 wt.% C). The cooling rate effect was studied by performing the quench at different cooling rates (-10, -50 and -100 °C/s) below Ms for each steel. A water-quenched condition was analyzed post-mortem by HEXRD too as well as by TEM and EBSD.

Conducting the mWH method coupled with a tetragonal lattice gives a tetragonal-corrected dislocation density. This new developed method gives results that differs of the conventional one but the difference falls into the precision of the method. As a consequence, it has been concluded that for low carbon martensitic steels, the correction could be neglected.

The retained austenite fraction decreases as lower the C content and faster the quenching.

The mean dislocation densities increase as the martensitic transformation progresses for all the studied conditions. It has been shown that the final dislocation density increases with the C content and that the obtained values are in accordance with the ones of the literature. This increase has been related to the higher volume variation associated with the transformation as carbon content increases. Although the effect of the cooling rate below Ms is not high for the studied cooling conditions, the much higher cooling rates in water-quenched samples lead to higher dislocation densities.

The spatial distribution of local dislocation density was quantified as well as the corresponding distribution of hardening due to dislocation density. The C content produces a small variation of the lowest value of the dislocation density strengthening but a significant increase of the dispersion of the mentioned distribution.

The results presented in this work reinforce the concept of the martensite as a microstructural based composite, which local yield strength dispersion becomes larger when the C content of the alloy increases.

Acknowledgements

This work was funded by the i-SITE Lorraine Université d'Excellence program (LUE) and supported by ArcelorMittal Maizières les Metz (Product Research Centre). The HEXRD experiments were conducted at DESY (PETRAIII-P07 beamline) in Hamburg under the I-20200450 EC grant. A special thanks is dedicated to the team of the P-07 line. The expertise of N. Schell and E. Maawad. was much appreciated and widely contributed to the success of the study.

This work was supported by the French State through the program "Investment in the future" operated by the National Research Agency (ANR) and referenced by ANR-11-LABX-0008-01 (LabEx DAMAS).

Patrick Barges and Mathieu Salib from ArcelorMittal Research SA are acknowledged for their help on the experiments and analyses. Jaafar Ghanbaja and Melanie Emo from the CC3M of the IJL are also acknowledged for the TEM measurements.

Conflicts of Interest

The authors declare no conflict of interest. The funders had no role in the design of the study; in the collection, analyses, or interpretation of data; in the writing of the manuscript, or in the decision to publish the results.

Data availability

The raw data required to reproduce these findings is shared at this.

Bibliography

[1] J. Lang, Study of the Metallography of Some Roman Swords, Britannia. 19 (1988) 199. https://doi.org/10.2307/526199.

[2] N. Fonstein, Advanced High Strength Sheet Steels: Physical Metallurgy, SPRINGER, 2015.

[3] C.C. Kinney, K.R. Pytlewski, A.G. Khachaturyan, J.W. Morris, The microstructure of lath martensite in quenched 9Ni steel, Acta Mater. 69 (2014) 372–385. https://doi.org/10.1016/j.actamat.2014.01.058.

[4] G. Krauss, Martensite in steel: strength and structure, Mater. Sci. Eng. A. 273–275 (1999) 40–57. https://doi.org/10.1016/S0921-5093(99)00288-9.

[5] H.K.D.H. Bhadeshia, Carbon in Cubic and Tetragonal Ferrite, Philos. Mag. Pap. Philos. Mag. 12 (2013) 3417–3429. https://doi.org/10.1080/14786435.2013.775518.

[6] P. Maugis, A Temperature–Stress Phase Diagram of Carbon-Supersaturated bcc-Iron, Exhibiting "Beyond-Zener" Ordering, J. Phase Equilibria Diffus. 41 (2020) 269–275. https://doi.org/10.1007/s11669-020-00816-2.

[7] J.K. Bowles, J.S.; Mackenzie, Crystallography of martensite transformations, Acta Metall. 2 (1954).

[8] L.-Å. Norström, O. Vingsbo, Influence of nickel on toughness and ductile-brittle transition in low-carbon martensite steels, Met. Sci. 13 (1979) 677–684. https://doi.org/10.1179/030634579790434321.

[9] H.K.D.H. Bhadeshia, C.H. Young, Strength of mixtures of bainite and martensite, Mater. Sci. Technol. 10 (1994) 209–214. http://www.maneyonline.com/doi/abs/10.1179/mst.1994.10.3.209.

[10] E.I. Galindo-Nava, P.E.J. Rivera-Díaz-Del-Castillo, A model for the microstructure behaviour and strength evolution in lath martensite, Acta Mater. 98 (2015) 81–93. https://doi.org/10.1016/j.actamat.2015.07.018.

[11] M. Kehoe, P.M.M. Kelly, The role of carbon in the strength of ferrous martensite, Scr. Metall. 4 (1970) 473–476. https://doi.org/10.1016/0036-9748(70)90088-8.

[12] L. Norström, The relation between microstructure and yield strength in tempered low-carbon lath martensite with 5% nickel, Met. Sci. 10 (1976) 429–436. https://doi.org/10.1179/030634576790431868.

[13] S. Morito, J. Nishikawa, T. Maki, Dislocation Density within Lath Martensite in Fe–C and Fe–Ni Alloys, ISIJ Int. 43 (2003) 1475–1477. https://doi.org/10.2355/isijinternational.43.1475.

[14] M. Shamsujjoha, Evolution of microstructures, dislocation density and arrangement during deformation of low carbon lath martensitic steels, Mater. Sci. Eng. A. 776 (2020) 139039. https://doi.org/10.1016/j.msea.2020.139039.

[15] T. Berecz, P. Jenei, A. Csóré, J. Lábár, J. Gubicza, P.J. Szabó, Determination of dislocation density by electron backscatter diffraction and X-ray line profile analysis in ferrous lath martensite, Mater. Charact. 113 (2016) 117–124. https://doi.org/10.1016/j.matchar.2015.11.014.

[16] Z.M. Shi, W. Gong, Y. Tomota, S. Harjo, J. Li, B. Chi, J. Pu, Study of tempering behavior of lath martensite using in situ neutron diffraction, Mater. Charact. 107 (2015) 29–32. https://doi.org/10.1016/j.matchar.2015.06.040.

[17] T. Ungár, S. Harjo, T. Kawasaki, Y. Tomota, G. Ribárik, Z. Shi, Composite Behavior of Lath Martensite Steels Induced by Plastic Strain, a New Paradigm for the Elastic-Plastic Response of Martensitic Steels, Metall. Mater. Trans. A Phys. Metall. Mater. Sci. 48 (2017) 159–167. https://doi.org/10.1007/s11661-016-3845-4.

[18] F. HajyAkbary, J. Sietsma, A.J. Böttger, M.J. Santofimia, An improved X-ray diffraction analysis method to characterize dislocation density in lath martensitic structures, Mater. Sci. Eng. A. 639 (2015) 208–218. https://doi.org/10.1016/j.msea.2015.05.003.

[19] J.L. Collet, M. Caruso, G. Lannoo, S. Cobo, S.M.C. van Bohemen, D. Ponge, C. Tasan, L. Morsdorf, L. Bracke, L. Moli Sanchez, New Metallurgical Tools for optimum design of modern Ultra High Strength Low Carbon Martensitic Steels, 2019. https://doi.org/10.2777/674520.

[20] L. Morsdorf, C.C. Tasan, D. Ponge, D. Raabe, 3D structural and atomic-scale analysis of lath martensite: Effect of the transformation sequence, Acta Mater. 95 (2015) 366–377. https://doi.org/10.1016/j.actamat.2015.05.023.

[21] S. Allain, O. Bouaziz, M. Takahashi, Toward a New Interpretation of the Mechanical Behaviour of As-quenched Low Alloyed Martensitic Steels, ISIJ Int. 52 (2012) 717–722. https://doi.org/10.2355/isijinternational.52.717.

[22] L.Y. Wang, Y.X. Wu, W.W. Sun, Y. Bréchet, L. Brassart, A. Arlazarov, C.R. Hutchinson, Strain hardening behaviour of as-quenched and tempered martensite, Acta Mater. (2020). https://doi.org/10.1016/j.actamat.2020.08.067.

[23] J. Macchi, S. Gaudez, G. Geandier, J. Teixeira, S. Denis, F. Bonnet, S.Y.P. Allain, Dislocation densities in a low-carbon steel during martensite transformation determined by in situ high energy X-Ray diffraction, Mater. Sci. Eng. A. 800 (2021) 140249. https://doi.org/10.1016/j.msea.2020.140249.

[24] T. Ungár, A. Borbély, The effect of dislocation contrast on x-ray line broadening: A new approach to line profile analysis, Appl. Phys. Lett. 69 (1996) 3173–3175. https://doi.org/10.1063/1.117951.

[25] J. Macchi, C. Couchet, C. Rampelberg, G. Geandier, Time-resolved dislocation density evolution during martensitic transformation tracked in situ by High-Energy XRD experiments: a study of C content and cooling rate effects - IJL, (2022). https://doi.org/doi:10.12763/SGPFMK.

[26] M. Humbert, L. Germain, N. Gey, E. Boucard, Evaluation of the orientation relations from misorientation between inherited variants: Application to ausformed martensite, Acta Mater. 82 (2015) 137–144. https://doi.org/10.1016/J.ACTAMAT.2014.09.007.

[27] J. Kieffer, G. Ashiotis, PyFAI: a Python library for high performance azimuthal integration on GPU, Powder Diffr. 28 (2014) 3. http://arxiv.org/abs/1412.6367 (accessed July 20, 2020).

[28] J. Rodríguez-Carvajal, Recent advances in magnetic structure determination by neutron powder diffraction, Phys. B Condens. Matter. 192 (1993) 55–69. https://doi.org/10.1016/0921-4526(93)90108-I.

[29] T. Ungár, G. Tichy, The effect of dislocation contrast on X-ray line profiles in untextured polycrystals, Phys. Status Solidi Appl. Res. 171 (1999) 425–434. https://doi.org/10.1002/(SICI)1521-396X(199902)171:2<425::AID-PSSA425>3.0.CO;2-W.

[30] S. Takaki, T. Masumura, T. Tsuchiyama, Proposal of simplified modified Williamson-Hall equation, ISIJ Int. 58 (2018) 2354–2356. https://doi.org/10.2355/isijinternational.ISIJINT-2018-517.

[31] G.. K. Williamson, W.. H. Hall, X-ray line broadening from filed aluminium and wolfram, Acta Metall. 1 (1953) 22–31. https://doi.org/10.1016/0001-6160(53)90006-6.

[32] A. Borbély, J. Dragomir-Cernatescu, G. Ribárik, T. Ungár, Computer program ANIZC for the calculation of diffraction contrast factors of dislocations in elastically anisotropic cubic, hexagonal and trigonal crystals, J. Appl. Crystallogr. 36 (2003) 160–162. https://doi.org/10.1107/S0021889802021581.

[33] S.Y.P. Allain, S. Gaudez, G. Geandier, J.C. Hell, M. Gouné, F. Danoix, M. Soler, S. Aoued, A. Poulon-Quintin, Internal stresses and carbon enrichment in austenite of Quenching and Partitioning steels from high energy X-ray diffraction experiments, Mater. Sci. Eng. A. 710 (2018) 245–250. https://doi.org/10.1016/j.msea.2017.10.105.

[34] Q. Liu, D. Juul Jensen, N. Hansen, Effect of grain orientation on deformation structure in cold-rolled polycrystalline aluminium, Acta Mater. 46 (1998) 5819–5838. https://doi.org/10.1016/S1359-6454(98)00229-8.

[35] Y. Nishi, M. Tachi, E. Yajima, Change in density of dislocations with cooling rate in liquid-quenched 18-8 stainless steel, Scr. Metall. 19 (1985) 865–866. https://doi.org/10.1016/0036-9748(85)90208-X.

[36] G.I. Taylor, Plastic Strain in Metals, J. Inst. Met. 62 (1938) 307-.

[37] G. Ghosh, G.B. Olson, The isotropic shear modulus of multicomponent Fe-base solid solutions, Acta Mater. 50 (2002) 2655–2675. https://doi.org/10.1016/S1359-6454(02)00096-4.

[38] K.W. Andrews, Heat Treatment for Improvement in Low Temperature Mechanical Properties of 0.40 pct C-Cr Steels., J. Iron Steel Inst. 203 (1965) 721.

[39] J. Wang, P.J. Van Der Wolk, S. Van Der Zwaag, Determination of martensite start temperature in engineering steels. Part I. Empirical relations describing the effect of steel chemistry, Mater. Trans. JIM. 41 (2000) 761–768. https://doi.org/10.2320/matertrans1989.41.761.

[40] S.M.C.C. Van Bohemen, Bainite and martensite start temperature calculated with exponential carbon dependence, Mater. Sci. Technol. 28 (2012) 487–495. https://doi.org/10.1179/1743284711Y.0000000097.

[41] D. Koistinen and R. Marburger, A general equation prescribing the extent of the austenite-martensite transformation in pure iron-carbon alloys and plain carbon steels, Acta Metall. 7 (1959) 59–60. https://doi.org/10.1016/0001-6160(59)90170-1.

[42] D.H. Sherman, S.M. Cross, S. Kim, F. Grandjean, G.J. Long, M.K. Miller, Characterization of the carbon and retained austenite distributions in martensitic medium carbon, high silicon steel, Metall. Mater. Trans. A Phys. Metall. Mater. Sci. 38 (2007) 1698–1711. https://doi.org/10.1007/s11661-007-9160-3.

[43] H. Godin, J.-D.D. Mithieux, C. Parrens, G. Badinier, M. Sennour, A.-F.F. Gourgues-Lorenzon, Effects of cooling path and resulting microstructure on the impact toughness of a hot stamping martensitic stainless steel, Mater. Sci. Eng. A. 742 (2019) 597–607. https://doi.org/10.1016/j.msea.2018.11.036.

[44] S. Gaudez, Kinetics and microstructural evolutions during the tempering of martensitic and nano-bainitic low alloyed steel: in situ experimental study and modelling, Université de Lorraine, 2021. http://www.theses.fr/2021LORR0016 (accessed February 17, 2022).

[45] Y. Wang, S. Denis, B. Appolaire, P. Archambault, Modelling of precipitation of

carbides during tempering of martensite, J. Phys. IV JP. 120 (2004) 103–110. https://doi.org/10.1051/jp4:2004120011.

[46] M. Hillert, The kinetics of the first stage of tempering, Acta Metall. 7 (1959) 653–658. https://doi.org/10.1016/0001-6160(59)90141-5.

[47] M. Hillert, L. Höglund, J. Ågren, Escape of carbon from ferrite plates in austenite, Acta Metall. Mater. 41 (1993) 1951–1957. https://doi.org/10.1016/0956-7151(93)90365-Y.

[48] L.C. Chang, H.K.D.H. Bhadeshia, Austenite films in bainitic microstructures, Mater. Sci. Technol. (United Kingdom). 11 (1995) 874–882. https://doi.org/10.1179/mst.1995.11.9.874.

[49] P. Retzl, S. Zamberger, E. Kozeschnik, Computational analysis of austenite film thickness and C-redistribution in carbide-free bainite, Mater. Res. Express. 8 (2021). https://doi.org/10.1088/2053-1591/ac0d6f.

Appendix A

Ms Temperatures

The Ms experimentally determined in the present work both by HEXRD vs dilatometry are compared in Figure 10, HEXRD values in the x axis and dilatometric values in the right y axis in blue. The sigma used around the experimental Ms HEXRD 1:1 ratio is equal to 10 °C. If the values obtained from both characterization technics are equal, then the blue dots would lie over the 1:1 line or in the confidence range (1:1 line ± 10 °C). The dilatometric values are systematically higher.

Different explanations might be postulated to explain the differences obtained from between the two characterization technics. Possible decarburization is often evoked but in our set-up in transmission, both technics would have been affected in a similar way if the XRD is performed (the data is obtained both from the center and the borders surface of the sample).

Our preferred explanation is that the HEXRD probe is focus on a local zone of the sample situated near the center of the 4x10 mm^2 surface of the sample, close to the thermocouple. On the contrary, the change of length measured by dilatometry corresponds to the is affected but the whole sample. This last measurement is affected by the known large temperature gradients in the long direction of the sample. The extremities of the sample touching the pods are systematically cooler that the bulk. may cool at a different rate. As a consequence, when cooling down the sample, the martensitic transformation could start at the extremities whereas the temperature at the center of the sample is not yet at the Ms temperatures. The change in length could then start before it could be detected by HEXRD. This gap width will naturally depends on the cooling rate and on the temperature itself.

Different empirical models are present in the literature for calculating the Ms temperature: the main substitutional elements are usually considered as well as the C content and in some recent models also the PAGS (Prior Austenite Grain Size). Two models with linear carbon dependency are used for the present comparison [38,39], one with exponential dependency [40] and another one that introduces the PAGS effect [19].

The Ms calculation equations based on a linear C dependency used in the present study are:

$$Ms(°C) = 539 - 423x_C - 30.4x_{Mn} - 17.7x_{Ni} - 12.1x_{Cr} - 7.5x_{Mo}$$ Andrews1965 [38]

$$Ms(°C) = 545 - 470.4x_C - 3.96x_{Si} - 37.7x_{Mn} - 21.5x_{Cr} - 38.9x_{Mo}$$ Wang2000 [39]

where x_i is the weight percentage of the alloying element i.

The Ms calculation equation based on a exponential C dependency used in the present study is:

$$Ms(°C) = 565 - \sum_i K_i x_i - 600[1-exp(-0.96\, x_C)]$$

$$with \sum_i K_i x_i = 31x_{Mn} + 13x_{Si} + 10x_{Cr} + 18x_{Ni} + 12x_{Mo}$$

Van Bohemen [40]

Finally, the utilized model with a relation between the Ms and the PAGS is:

$$Ms(°C) = T_1 - \frac{1015 + W_\mu + 370\exp\left(-\frac{6D_\gamma}{11}\right) + 350/\sqrt{D_\gamma}}{7.22}$$

$$with \quad T_1 = 718.3 - 291x_C - 24x_{Mn} - 1.8x_{Si} - 5.6x_{Cr} - 18.4x_{Ni} + 3.5x_{Mo}$$ ToolMart [19]

$$and \quad W_\mu = 670x_C^{0.5} + \sqrt{\frac{\left(195x_{Mn}^{0.5}\right)^2 + \left(140x_{Si}^{0.5}\right)^2 + }{\left(170x_{Cr}^{0.5}\right)^2 + \left(5x_{Ni}^{0.5}\right)^2 + \left(205x_{Mo}^{0.5}\right)^2}}$$

The calculated Ms are presented in Figure 10 in black points. As previously explained, a well correlation between the Ms determined by HEXRD and the calculated ones is found when the points corresponding the calculated values are close to the black line corresponding to the 1:1 ratio.

The values predicted by the model proposed by Andrews [38] and Van Bohemen [40] are in better accordance with Ms determined by dilatometry, while the ToolMart [19] and Wang [39] models results are closer to the HEXRD Ms. This might be explained by the dataset used in each case for calibrating the authors model, if the model are calibrated with Ms determined by dilatometry or XRD characterization technics.

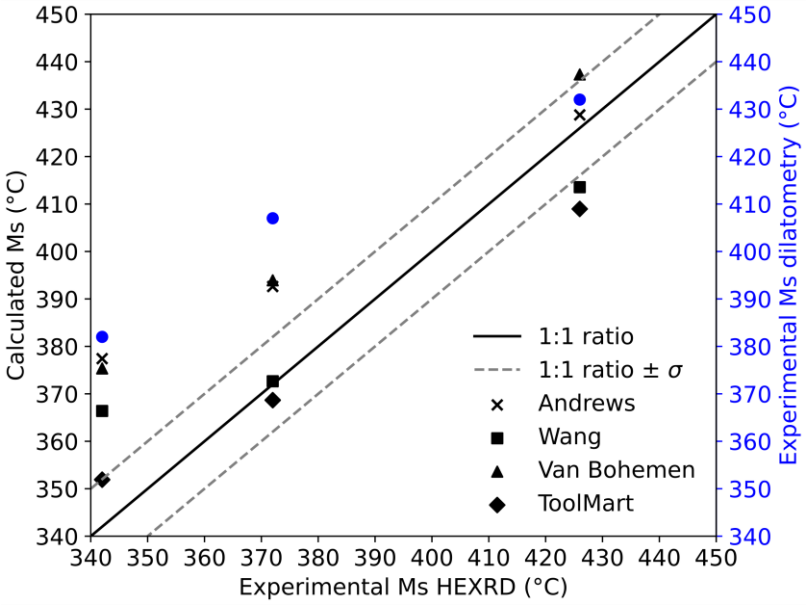

Figure 10: Correlation between experimentally determined Ms (by dilatometry (blue points) and HEXRD (1:1 ratio black line) and the predicted ones [19,38–40] (Color online).

Appendix B

Retained austenite at room temperature

The measured retained austenite fractions presented in Table 4 show an increase of retained austenite with the C content. This effect can be directly explained by the related evolution of the Ms temperature with the C content and the Koistinen-Marburger equation [41]. The effect of the cooling rates is less common but has already been reported by Sherman et al. [42] and by Godin et al. [43].

At least two different phenomena have to be considered to explain the stabilization of austenite, the first one is the internal stresses stabilization, the second one is the chemical stabilization. The stabilization due to the compressive state produced in austenite by the displacive transformation martensitic transformation (as it has been evidenced in several previous studies by HEXRD, as in page 74 of [44]) could increase at higher cooling rates (as lower relaxation is expected) while the chemical stabilization due to carbon partition is supposed to have a more important effect for lower cooling rates. For lower cooling rates, the carbon, trapped in the ferrite matrix during the displacive transformation, could diffuse into the austenite increasing its stability as proposed by Sherman et al. [42] following a partitioning mechanism.

This last hypothesis can be assessed by calculating the average C diffusion distance $<\sqrt{Dt}>$ within a martensite formed at a given temperature for the different cooling paths. In the case of a martensite formed at 320 °C and following cooling paths of -10, -50 and -100 °C/s until 200 °C the average C diffusion distance are 1.1, 0.21 and 0.11 μm respectively, considering D_0=2.0e6 and Q=-108000 J/mol [45,46]. Taking into account that at 320 °C 50 wt.% martensite has been already transformed, and the already mentioned PAGS, C atoms can reach non-transformed austenite regions considering the lower cooling rate.

This calculation is consistent with the previous work of Hillert et al. [47] who also studied the partition of carbon from ferrite plates into austenite and their results show that for a 0.4 wt.% C steel after around 0.1s at 350 °C at least 75% of C can been segregated into austenite considering a distance of 0.2 μm. The C segregation from ferrite/martensite platelets into neighboring austenite is addressed in several works studying the bainitic transformation and the austenitic stabilization [48,49]. Thus, chemical stabilization of austenite by C partitioning is possible during quench at not high enough cooling rates. It has to be kept in mind that if the cooling rate is low enough self-tempering cannot be ruled out and not all the carbon will be available to segregate into the austenite.

A third phenomenon that cannot be ruled out is that faster cooling rate may boost the autocatalytic formation of the martensite producing lower fraction of retained autenite.